

PAPER • OPEN ACCESS

Dynamic speckle imaging with SVD compression

To cite this article: E. Stoykova *et al* 2022 *J. Phys.: Conf. Ser.* **2407** 012049

View the [article online](#) for updates and enhancements.

You may also like

- [Fabrication of silver nanostructures using femtosecond laser-induced photoreduction](#)
Peter Barton, Sanjoy Mukherjee, Jithin Prabha *et al.*
- [SOFIA, an airborne observatory for infrared astronomy](#)
Alfred Krabbe, Dörte Mehlert, Hans-Peter Röser *et al.*
- [Impact of equatorial and continental airflow on primary greenhouse gases in the northern South China Sea](#)
Chang-Feng Ou-Yang, Ming-Cheng Yen, Tang-Huang Lin *et al.*



Breath Biopsy[®] OMNI[®]

The most advanced, complete solution for global breath biomarker analysis

TRANSFORM YOUR RESEARCH WORKFLOW



Expert Study Design & Management



Robust Breath Collection



Reliable Sample Processing & Analysis



In-depth Data Analysis



Specialist Data Interpretation

Dynamic speckle imaging with SVD compression

E. Stoykova¹, M. Levchenko¹, B. Ivanov¹, V. Madjarova¹, D. Nazarova¹,
L. Nedelchev¹, A. Machikhin², J. Park³

¹Institute of Optical Materials and Technologies, Bulgarian Academy of Sciences,
Acad. Georgi Bonchev Str., Bl.109, 1113 Sofia, Bulgaria

²Scientific and Technological Center of Unique Instrumentation, Russian Academy of
Sciences, 15 Butlerova, Moscow, 117342, Russia

³Electronics and Telecommunications Research Institute, 218 Gajeong-ro, Yuseong-
gu, Daejeon, 34129, Republic of Korea

mialevchenko@gmail.com

Abstract. Dynamic speckle imaging (DSI) of areas with different speed of processes ongoing in industrial or biological objects relies on statistical processing of a large number of images of the speckle patterns formed on the objects surface under laser illumination. The DSI visualizes the speed spatial distribution as an activity map. We propose compression of the raw DSI data by applying singular value decomposition (SVD). A specific feature of speckle images for DSI is lack of a structure with areas of close intensity values. The gain from the direct SVD application may be modest in cases when a great number of non-zero singular values is needed to build an activity map comparable in quality to the ground truth map from bitmap images. For higher compression, we propose SVD to be applied to the 2D arrays containing the differences between the successive images. The SVD compression has been verified by using synthetic and experimental data.

1. Introduction

Intensity-based dynamic speckle imaging (DSI) produces a 2D map of activity through statistical processing of speckle patterns [1,2] formed on the surface of industrial or biological objects under laser illumination. The activity map gives areas of different speed of processes ongoing in the objects. The potential of the DSI has been proven for various applications as monitoring of blood flow in human tissues [3-5], analysis of seeds viability [6,7], plants growth, chemical contamination of leaves [8,9], penetration of cosmetic ingredients in human skin [10], study of ear biometrics [11], bacterial response [12,13] and animal reproduction [14], food quality assessment [15-17], observation of a drying process [18,19] and fire detection [20] to name a few.

The DSI is highly sensitive to micro-changes of the object topography or to variations in the refractive index in the light beam in time at the expense of strong fluctuations of the activity map entries. For a high-quality map, storage and processing of a large number of images is required. Accordingly, raw data compression becomes mandatory for monitoring a process in time when many maps are built at consecutive instants. The raw data are 8-bit encoded images of correlated in time speckle patterns. They represent widely spread within the dynamic range of the optical sensor symmetric/asymmetric intensity distributions with a signal-dependent variance in the general case of non-uniform illumination or varying surface roughness. Spatial correlation between the intensity values is very low.



Compression of images of speckle patterns must keep intact information carried by the activity map about the speed of intensity changes in time. Speed analysis relies on the rate of temporal variation of the recorded intensity values and not on the intensities themselves. This allowed us to propose coarse quantization [21] or binarization [22] as approaches for reducing volume of the speckle data. Furthermore, we proved efficiency of different JPEG compression formats applied to speckle images [23] although blocking or other artefacts were observed on the activity maps at low quality of decompressed images or high compression ratio.

In this work, we consider another type of lossy compression of the raw DSI data by applying a singular value decomposition (SVD) to the images of the speckle patterns. Several decomposition approaches have been recently reported for processing of sequences of dynamic speckle patterns. An empirical mode decomposition was introduced to evaluate different activity levels in the time–frequency plane [24]. Some limitations of this method were removed later by using a variational mode decomposition [25]. The SVD was used for spatio-temporal characterization of activity by dividing speckle images into blocks [26]. Contrary to these approaches, aiming at activity evaluation, we propose to use the SVD not for processing of the speckle patterns but for their compression. In our approach, the DSI is implemented according to the following scheme: i) recording of N correlated in time speckle images for a single activity map; ii) SVD compression of the images and storage of non-zero data; iii) calculation of activity map from decompressed images built from the non-zero data. The benefit from compression is the option to perform step 3 at any appropriate time after the acquisition.

We propose two ways of implementation of the SVD compression. The first option is direct application of the SVD method to the recorded images. A specific feature of speckle images in the DSI is lack of a structure with areas comprising close intensity values. Thus, the gain from the direct SVD application to the recorded images may be rather modest because a comparatively great number of non-zero singular values should be kept to obtain an activity map comparable in quality to the ground truth map built from bitmap images. That's why for higher compression, we propose the second option of SVD when it is applied to the 2D arrays containing the differences between the successive images in the recorded sequence. The SVD compression is verified by using synthetic and experimental data.

2. SVD compression of synthetic speckle images

2.1. Generation of synthetic images

To introduce the SVD compression problem in DSI, we consider the case of pointwise processing of speckle images captured for a synthetic flat object with four equal in size regions A1, A2, A3, A4 of different activity (Fig.1). Activity at point (x, y) is characterized by correlation radius, $\tau_c(x, y)$, of the normalized temporal correlation function $\rho_{xy}(\tau)$ of intensity fluctuations in time at this point; τ is the time lag. We generated N speckle images of size $N_x \times N_y$ pixels at a frame rate $1/\Delta t$, where Δt is the time interval between two successive images. The size corresponding to each activity region was $N_x \times 0.25N_y$. The values of τ_c in the regions A1, A2, A3, A4 are equal to $10\Delta t$, $20\Delta t$, $40\Delta t$, $80\Delta t$ respectively.

Simulation procedure (described in detail in [27]) included generation of correlated wrapped phase distributions on the object surface at consecutive instants for illumination at wavelength, λ . The formed complex amplitudes were further propagated to the camera aperture through an objective lens. The diameter and the focal distance of the lens determine the distribution of intensity in the recorded images. Generation started with a 2D array of random delta-correlated phase values uniformly distributed from 0 to 2π . For movement of the scattering centers normally to the object surface, the phase is a normally distributed quantity. The additional assumption is that the amplitudes and phases of the scattered light are mutually independent at each scattering center and between any two centers. We simulated the case of uniform illumination and equal reflectivity across the object. Simulation was done for $\rho_{xy}(\tau) = \exp(-\tau/\tau_c)$ as a correlation function describing various processes. The standard deviation of the phase change between successively acquired images is $\sigma_\phi = N(0,1)\sqrt{\Delta t/\tau_c(x,y)_c}$, where $N(0,1)$ is a

random number with normal distribution with a zero mean and a standard deviation equal to 1. Integration of speckle by the camera pixels was also modeled.

We generated speckle patterns of size 512×512 pixels at wavelength 532 nm. One of them is shown in Fig.1. Speckle obeys the same intensity distribution at all pixels. To detect higher or lower activity at point $(x = i\Delta, y = k\Delta)$, where Δ is the pixel interval, processing of the sequence of intensities $I_{ik,n}, n = 1 \dots N$ is required.

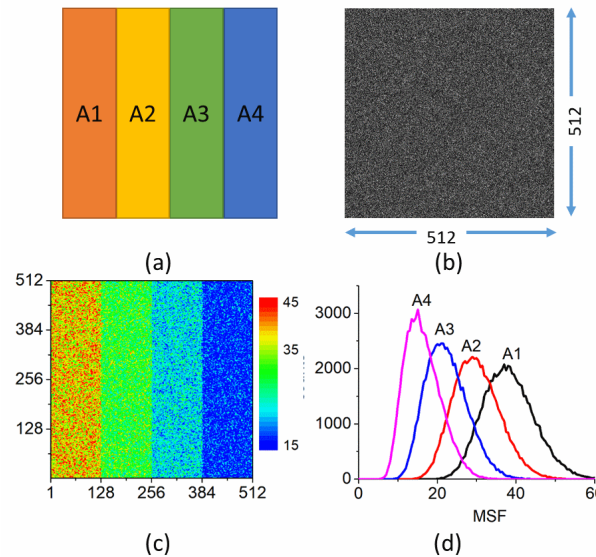


Figure.1. Synthetic object with 4 activity regions (a) and its speckle image (b); an activity map built from 256 speckle images of the object at time lag $\tau = 10\Delta t$ (c) and the histograms of the MSF estimate in the four object regions (d).

We estimated activity by using a modified structure function (MSF) [27]:

$$\hat{S}_1(i, k, m) = \frac{1}{N} \sum_{n=1}^{N-m} |I_{ik,n+m} - I_{ik,n}| \quad (1)$$

where $m = \tau/\Delta t$. The map obtained at $\tau = 10\Delta t$ from 256 8-bit encoded bmp images is presented in Fig.1(c). This ground truth map clearly visualizes the four regions of activity. The faster the process, the higher the MSF values. The MSF estimate fluctuates from point to point. The number of pixels in one activity region is $512 \times 128 = 65536$. This number of entries allows to build a histogram which rather accurately represents the probability density function (PDF) of the estimate (1) at a given activity. The histograms of the MSF estimate in the four activity regions are shown in Fig.1(d). They are rather wide but overlap only partially which is the reason for the good contrast of the activity map.

2.2. Direct SVD compression of speckle images

SVD was applied to each image $I_n = \{I_{ik,n}; i = 1 \dots N_x, k = 1 \dots N_y\}$ in the sequence of images, $I_1, I_2 \dots I_N$. Each speckle image is represented as a product of three matrices, $I_n = U_n \Sigma_n V_n^T$, and only Q non-zero singular values were kept in all diagonal matrices $\Sigma_n, n = 1 \dots N$. As a result, a sequence of decompressed images is formed as $J_n = U_n' \Sigma_n' V_n'^T, n = 1 \dots N$, where U_n' is composed from the first Q columns of U_n and V_n' - from the first Q rows of V_n ; the size of the diagonal matrix Σ_n' is $Q \times Q$. The size of each recorded image in the sequence $I_1, I_2 \dots I_N$ is $N_x \times N_y$. We calculated the activity maps from the decompressed images $J_1, J_2 \dots J_N$ corresponding to different number of modes, Q , and found the mean values and the standard deviations of the MSF estimate (1) in the four activity regions. The results are shown in Fig.2. The last points in the plots at $Q = 512$ correspond to the case of non-compressed bmp images. Compression is achieved at Q less than 256. We see that comparatively high compression at

small number of non-zero modes leads to substantial decrease of the differences between the mean values. In parallel, standard deviation is also decreasing, but the final result is that the contrast of the activity maps at small Q is rather low.

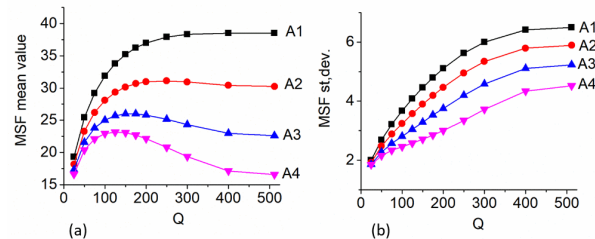


Figure. 2 Mean values (a) and standard deviations (b) of the MSF estimate in the four activity regions of the synthetic object in Fig.1 as a function of the number of non-zero modes, Q ; time lag $\tau = 10\Delta t$, $N = 256$.

The low contrast is a serious drawback, as one may see in Fig.3 which presents the maps obtained from the decompressed images J_1, J_2, \dots, J_N at $Q = 25, 50, 100$ and 150 . The maps at $Q = 25$ and 50 are of little use for the dynamic speckle analysis. In addition, they exhibit also some artefacts. The maps at $Q = 100$ and 150 are acceptable, especially if some contrast enhancement technique is applied. Note that the maps in Fig.3 are plotted for the same colour scale as for the ground truth map in Fig.1 for better comparison.

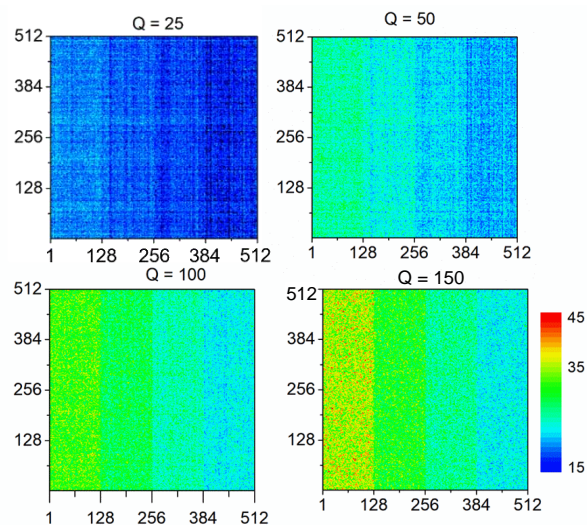


Figure.3. Activity maps for a synthetic object with 4 activity regions at different compression ratios: 10.24 ($Q = 25$), 5.12 ($Q = 50$), 2.56 ($Q = 100$), 1.7 ($Q = 150$); time lag $\tau = 10\Delta t$, $N = 256$.

The last conclusion is supported also by the histograms of the MSF estimate in Fig.4 at different Q values. The histograms are given within the same interval of the MSF values and the same size of the bin as in Fig.1 for better comparison. As Q is decreasing, the histograms become narrower, so the fluctuations of the estimate decrease in their spread, but the overlap is rather substantial. We see that Q must be equal or greater than 100, so the gain from the SVD compression in the analysed case of a gray-scale image is rather modest (approximately 3 times).

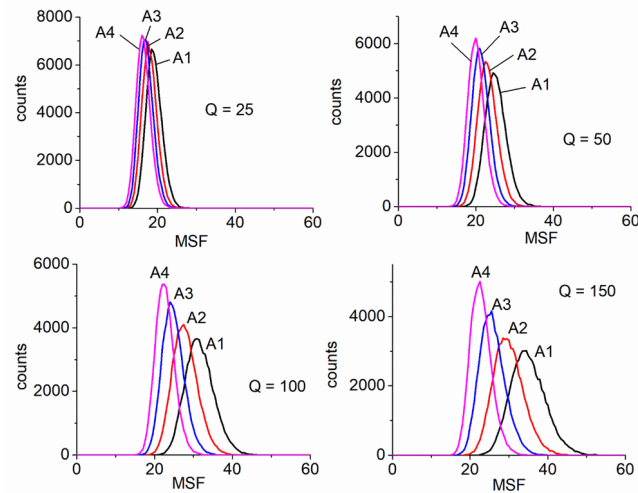


Figure.4. Histograms of the MSF estimate for a synthetic object with 4 activity regions at different compression ratios: 10.24 ($Q = 25$), 5.12 ($Q = 50$), 2.56 ($Q = 100$), 1.7 ($Q = 150$); time lag $\tau = 10\Delta t$, $N = 256$.

2.3. Image difference SVD compression

As it is seen in Fig.1(b), speckle images, which are input data for the processing algorithm, are grainy images without structure, and SVD approach is less effective. For better SVD compression, we proposed to compress the differences, $D_n = I_{n+1} - I_n$, $n = 1 \dots N - 1$. The arrays D_n , $n = 1 \dots N - 1$ exhibit some structure due to the spatial distribution of the speed of the ongoing processes. The activity maps and the histograms of the MSF estimate, that have been built at time lag $\tau = 10\Delta t$, $N = 25$ for a sequence $D'_1, D'_2 \dots D'_{N-1}$ restored after SVD compression of $D_1, D_2 \dots D_{N-1}$, are shown for $Q = 10, 25, 50$ in Fig. 5 and Fig.6 respectively.

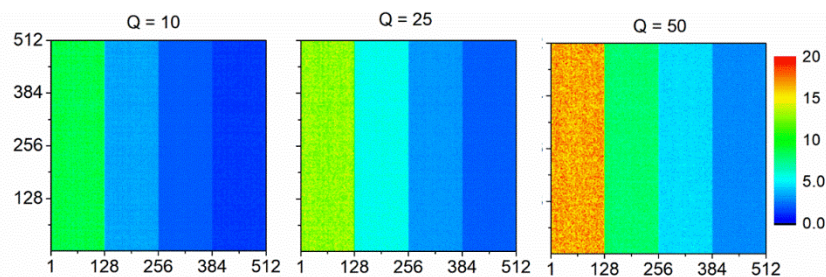


Figure.5. Activity maps for a synthetic object with 4 activity regions at different compression ratios: 25.06 ($Q = 10$), 10.24 ($Q = 25$), 5.12 ($Q = 50$); time lag $\tau = 10\Delta t$, $N = 256$.

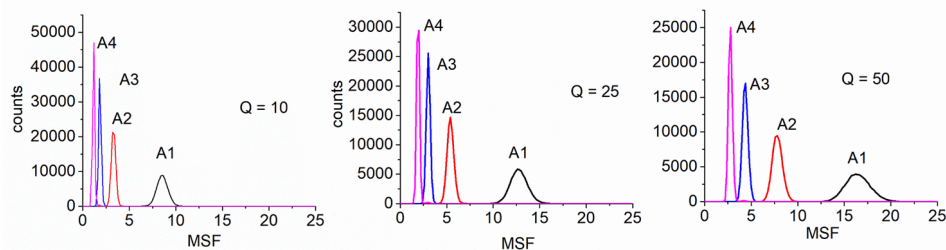


Figure.6. Histograms of the MSF estimate for a synthetic object with 4 activity regions at different compression ratios: 25.06 ($Q = 10$), 10.24 ($Q = 25$), 5.12 ($Q = 50$); time lag $\tau = 10\Delta t$, $N = 256$.

The obtained maps show very good contrast because the histograms of the MSF estimate do not overlap. Decrease of Q leads to decrease of the mean values of the estimate and the spread of the histograms. As it should be expected, the spread is the largest for the region A1 with the fastest fluctuations of intensity. The activity areas can be easily distinguished even at $Q = 10$. In view that SVD compression inevitably leads to changes in spatial correlations between the intensity data in the decompressed images, the second SVD approach is more appropriate for objects with comparatively large activity regions.

3. SVD compression of experimental speckle images

For the experimental check of feasibility of SVD compression of speckle images acquired for the DSI, we chose two objects: i) a Bulgarian coin of 1 Lev covered with a non-transparent paint and ii) a water polymer solution droplet spread on a glass substrate. Activity in the first object was produced by different evaporation rate of the paint in the coin's grooves, embossment and flat surface. Evaporation of the polymer solution was monitored by recording series of images at different time offsets, t_0 , from the beginning of the experiment. We used azopolymer poly [1- [4- (3-carboxy-4-hydroxy-phenylazo) benzene-sulfonamido] -1,2-ethanediyl, sodium salt] with abbreviation PAZO from Sigma Aldrich. We used color CMOS camera X06c-s (Baumer) with 780×582 pixels at pixel pitch $8.3 \mu\text{m}$, exposure time $20 \mu\text{sec}$ at Δt equal to 250 msec. A linearly polarized light from a He-Ne laser emitting at 632.8 nm illuminated the objects on a vibration-isolated table. Polarization was checked with PAX5710VIS-T polarimeter (Thorlabs). Exemplary speckle images recorded for the two objects are presented in Fig.7. As is seen, speckle entirely obscures the coin's relief. The same is valid for the polymer droplet. The drying process created evolving in time and space distribution of activity.

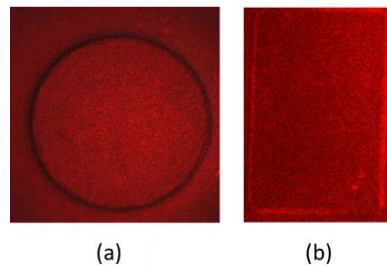


Figure.7. Speckle patterns for a coin covered with a non-transparent paint (a) and a droplet of a polymer solution on a glass substrate (b); wavelength 632.8 nm .

The ground truth map and the activity maps obtained from image sequence $J_1, J_2 \dots J_N$ with increasing number of modes, Q , at $N = 256$ and a time lag $\tau = 10\Delta t$ are shown in Fig.8 for the test object coin. The maps are plotted with the same scale. The maps were obtained by using a normalized MSF processing:

$$\hat{S}_2(i, k, m) = \frac{1}{N\hat{v}_{ik}^{1/2}} \sum_{n=1}^{N-m} |I_{ik,n+m} - I_{ik,n}| \quad (2)$$

where $\hat{v}_{ik} = N^{-1} \sum_{n=1}^N (I_{ik,n} - \hat{I}_{ik})^2$ and $\hat{I}_{ik} = N^{-1} \sum_{n=1}^N I_{ik,n}$ are the estimates of the variance and the average intensity at point $(i\Delta, k\Delta)$. The number of the used pixels in the color RGB images was 580×600 , so the total number of the recorded intensity values in the three channels was $3 \times 580 \times 600$. We used this number to evaluate the compression ratio when only $Q(1 + N_x + N_y) = 1181Q$ non-zero values are kept.

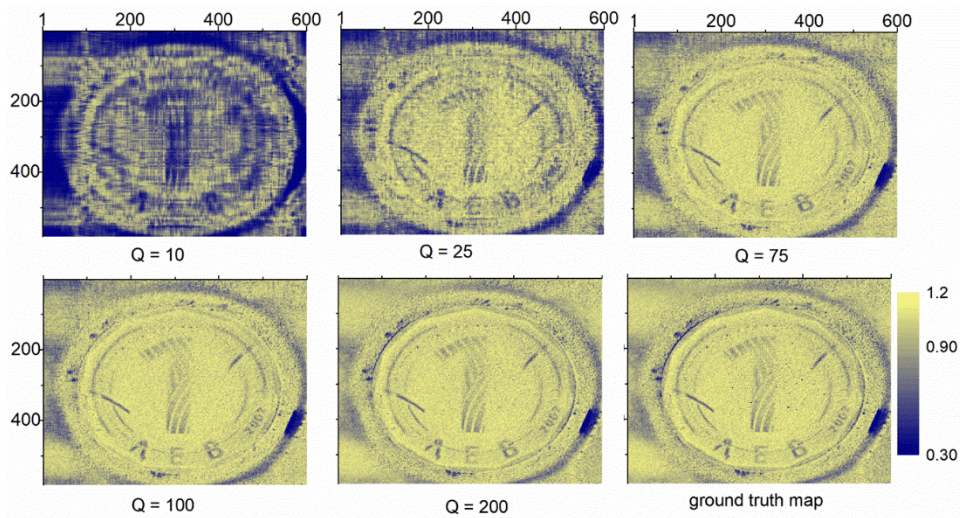


Figure.8. Activity maps for a coin covered with non-transparent paint at different compression ratios: 88.4 ($Q = 10$), 41.8 ($Q = 25$), 11.8 ($Q = 75$), 8.8 ($Q = 100$), 4.4 ($Q = 200$); time lag $\tau = 10\Delta t$, $N = 256$.

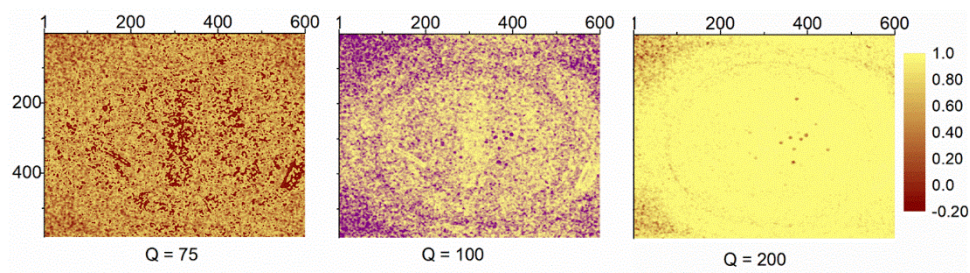


Figure.9. Structural similarity maps for the ground truth map of MSF estimate (2) for a coin covered with non-transparent paint and activity maps at different compression ratios: 11.8 ($Q = 75$), 8.8 ($Q = 100$), 4.4 ($Q = 200$); time lag $\tau = 10\Delta t$, $N = 256$.

As is seen, the activity maps resemble an image of the coin relief with increasing quality as Q is increasing. The maps are acceptable for $Q \geq 75$. The maps of the structural similarity index between the ground truth activity map and the map from decompressed $J_1, J_2 \dots J_N$ images for $Q = 75, 100$ and 200 are presented in Fig.9. According to the maps in Fig.9, the result is acceptable at $Q \geq 100$.

Figure 10 presents the activity maps obtained from the sequence $D'_1, D'_2 \dots D'_{N-1}$ composed at $Q = 50$ from the speckle images acquired for the second object. The time lag was $\tau = 10\Delta t$ and $N = 256$. The maps correspond to the MSF estimate (1). As it should be expected, the mean values of the estimate for the maps from the decompressed images are lower than for the ground truth maps. The maps at $Q = 50$ are smoother than the ground truth maps. In both cases, decrease of activity due to the drying is visible. Compression for $Q = 50$ is about 20 times.

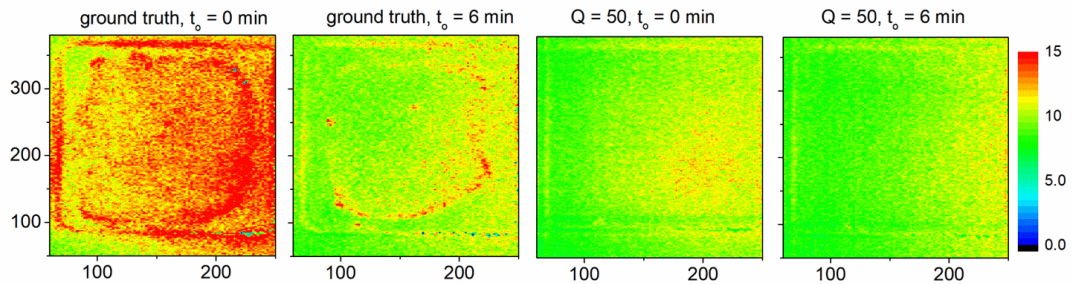


Figure.10. Ground truth map and activity map at $Q = 50$ for a droplet of polymer solution at the beginning of the experiment and at 6 minutes after; the maps are calculated by processing arrays of differences of successive images at time lag $\tau = 10\Delta t$, $N = 256$.

4. Conclusion

In summary, we proved feasibility of SVD compression for the dynamic speckle measurement of speed of processes ongoing in industrial or biological objects. The output of the measurement is a set of 2D activity maps computed at different instants to visualize the speed spatial evolution. We proposed two ways to apply SVD and verified them for synthetic and experimental images. The first one decomposes the recorded speckle images, and the second one decomposes the arrays containing the difference between the intensity values in consecutive images. The first approach requires a larger number of non-zero singular values but it provides better spatial resolution in building the activity map. This has been clearly seen from the good quality of the activity maps obtained for a test object coin covered with a non-transparent paint. The second approach provides high quality of the activity map at smaller number of non-zero singular values, and compression substantially increases. The proposed second SVD compression was verified by a polymer drying experiment. It is feasible for objects with larger areas of constant activity. The SVD method is suitable also for non-uniform illumination with normalized processing.

Acknowledgements.

The reported study was funded by the joint project of the National Science Fund of Bulgaria (contract KII-06-Russia/7) and the Russian Foundation for Basic Research (contract #20-58-18007) as well as by IITP grant funded by the Korea government (MSIT) (№. 2019-0-00001, Development of Holo-TV Core Technologies for Hologram Media Services). E. Stoykova thanks European Regional Development Fund within the Operational Programme “Science and Education for Smart Growth 2014–2020” under the Project CoE “National center of Mechatronics and Clean Technologies” BG05M2OP001-1.001-0008. M. Levchenko thanks 2020 Plenoptic Imaging H2020 Marie Skłodowska-Curie Innovative Training Network, project № 956770.

References

- [1] Goodman J 2007 *Speckle Phenomena in Optics: Theory and Applications* (Roberts and Company Publishers)
- [2] Rabal H J and Braga R A Jr 2009 *Dynamic Laser Speckle and Applications* (CRC Press).
- [3] Fujii H, Nohira K, Yamamoto Y, Ikawa H and Ohura T 1987 *Appl. Opt.* **26** 5321–5
- [4] Serov A and Lasser T 2005 *Opt. Express* **13** 6416–28
- [5] Rajan V, Varghese B, van Leeuwen T and Steenbergen W 2006 *Opt. Lett.* **31** 468–70
- [6] Braga R, Fabbro I, Borem F, Rabelo G, Arizaga R, Raba H and Trivi M 2003 *Biosystems Eng.* **86**,287-94
- [7] Braga R, Rabelo G, Granato L, Santos E, Machado J, Arizaga R, Rabal H and Trivi M 2005 *Biosystems Eng.* **91** 465-9
- [8] Braga R A, Dupuy L, Pasqual M and Cardoso R R 2009 *Eur.Biophys. J.* **38** 679–86

- [9]. Ivanov B, Stoykova E, Berberova N, Nikova T, Krumov E and Malinowski N 2013 *Bulg. Chem. Commun.* **45** 149 – 53
- [10] Stoykova E, Blagoeva B, Nazarova D, Nedelchev L, Nikova T, Berberova N, Kim , and Kang H 2018 *Opt. Quant. Electron.* **50** 191-201
- [11] Chatterjee A, Singh P, Bhatia V and Prakash S 2019 *Opt. Las. Technol.*, **112** 368-78
- [12] Murialdo S E, Sendra G H, Passoni L I, Arizaga R, Gonzalez J F, Rabal H and Trivi M 2009 *J. Biomed. Opt.* **14** 064015
- [13] Mandracchia B, Palpacuer J, Nazzaro F, Bianco V, Rega R, Ferraro P 2018 *IEEE J. Selected Topics in Quant. Electron.* **25** 1-6
- [14] Macedo R, Barreto Filho J, Braga R Jr, Rabelo G 2009 *Reprod. Fertil. Dev.* **22** 170–1
- [15] Ansari M Z, Minz P D and Nirala A K 2012 *Proc. IEEE Conf. on Recent Advances in Information Technology (IEEE)* 873–6
- [16] Mulone C, Budini N, Vincitorio F, Freyre C, López Díaz A and Ramil Rega O 2013 *Proc. SPIE* **8785**, 87851X
- [17] Lyubenova T, Stoykova E, Nacheva E, Ivanov B, Panchev I and Sainov V 2013 *Proc. SPIE* **8770**, 87700S
- [18] Harizanova R, Gaydarov V, Zamfirova G, Stoykova E, Nazarova D, Blagoeva B and Nedelchev L 2019 *Thin Solid Films* **687** 137441
- [19] Martí-López L, Cabrera H, Martínez-Celorio R A and González-Peña R 2010 *Opt. Commun.* **283** 4972-7
- [20] Christensen C, Zainchkovskyy Y, Barrera-Figueroa S, Torras-Rosell A, Marinelli G, Sommerlund-Thorsen K, Kleven J, Kleven K, Voll E, Petersen J and Lassen M 2019 *Appl. t.* **58** 7760-65
- [21] Stoykova E, Nazarova D, Nedelchev L, Ivanov B, Blagoeva B, Oh K and Park J 2020 *Appl. Opt.* **59** 2810-19
- [22] Stoykova E, Kang H, Kim Y, Nazarova D, Nedelchev L, Ivanov B, Berberova N and Mateev G 2018 *Opt. Las. Eng.* **111** 50-57
- [23] Stoykova E, Blagoeva B, Berberova-Buhova N, Levchenko M, Nazarova D, Nedelchev L and Park J 2022 *Appl. Opt.* **61** B287-96
- [24] Federico A, Kaufmann G 2006 *Optics Commun.* **267** 287-94
- [25] Tang X, Zhong P, Li Z, Gao Y, Hu H 2021 *Optik* **243** 167475
- [26] Kulkarni R, Pal P, Banoth E 2021 *Opt. Las. Eng.* **142** 106588
- [27] Stoykova E, Nazarova D, Berberova N and Gotchev A 2015 *Opt. Express* **23** 25128-42